ELSEVIER

International Journal of Solids and Structures 41 (2004) 785–800

INTERNATIONAL JOURNAL OF SOLIDS and STRUCTURES

www.elsevier.com/locate/ijsolstr

Experimental and numerical analyses of PCC overlays on PCC slabs-on-grade subjected to climatic loading

Seong-Min Kim [a,*], Patricia Kim Nelson [b,1]

[a] *Center for Transportation Research, The University of Texas at Austin, 3208 Red River, Suite 200, Austin, TX 78705, USA*
[b] *The Transtec Group, Inc., 1012 E. 38 1/2 St., Austin, TX 78751, USA*

Received 29 May 2003; received in revised form 28 September 2003

Abstract

Most distresses in composite pavement structures, such as Portland cement concrete (PCC) overlays on PCC slabs-on-grade, form when their layers delaminate. To predict the delamination potential of bonded concrete overlays (BCOs) on slab-on-grade pavements at early ages, a mechanistic delamination model was developed in this study. To calibrate the model, an experimental BCO on jointed concrete pavement (JCP) section was constructed, and its behavior was monitored for the first 72 h after construction when subject to climatic loading, i.e. changes in temperature and moisture. Two- and three-dimensional finite element models of the BCO system were developed and calibrated. Theoretical equations to predict the corner stresses at the interface were formulated using the interfacial stresses predicted by the two-dimensional model as input. These equations yield stresses that match the results from the three-dimensional model well. A sensitivity analysis reveals the influence of overlay and JCP parameters, such as elastic modulus, slab length, thickness, and coefficient of thermal expansion, on the interfacial shear and normal stresses. This mechanistic delamination model has been incorporated into the HIPERBOND software developed for the Federal Highway Administration.

Keywords: Bond; Climatic loading; Delamination; Early age; Finite element; Interfacial stress; Jointed concrete pavement; Overlay; Portland cement concrete

1. Introduction

One of the primary assumptions in the design of bonded concrete overlays (BCOs) is that a sound bond exists between the overlay and the existing pavement, thereby creating a composite structure. If this bond deteriorates, the pavement will most likely not perform as intended and distresses, such as cracks and punchouts, will form. Bond failure, also called delamination, is the precursor to distress formation on many BCO projects. Repair of the distresses come at a great expense, as has been seen numerous times in the field.

* Corresponding author. Tel.: +1-512-232-3134; fax: +1-512-232-3151.
E-mail addresses: seong-min@mail.utexas.edu (S.-M. Kim), pknelson@thetranstecgroup.com (P. Kim Nelson).
[1] Tel.: +1-512-451-6233; fax: +1-512-451-6233.

0020-7683/$ - see front matter © 2003 Elsevier Ltd. All rights reserved.
doi:10.1016/j.ijsolstr.2003.10.013

Because of this, one of the primary objectives of the pavement designer is to prevent interfacial delamination of bonded Portland cement concrete (PCC) overlays on PCC slabs-on-grade. Delamination is often due to an inadequacy in one (or more) pavement design variables: the pavement design, the Portland cement materials and mix design, the climatic conditions at the time of construction, and the methods of construction. This led the Federal Highway Administration (FHWA) to develop guidelines for the design and construction of BCOs (McCullough and Rasmussen, 1999a). FHWA's HIPERPAV software package was developed in the 1990s to predict the early-age behavior of jointed concrete pavements (JCPs) based on input from the pavement design variables listed above (McCullough and Rasmussen, 1999a,b). HIPERBOND (*Hi*gh *Per*formance *Bond*ed Concrete Overlays) is an analysis module contained in HIPERPAV. The HIPERBOND module focuses on predicting the delamination potential of BCOs on JCPs. The development of HIPERBOND is important since BCOs on JCPs are a commonly used rehabilitation technique.

One objective of this study is to develop and calibrate a mechanistic delamination model for BCOs on JCPs and to integrate it into the HIPERBOND software module. The other objective is to investigate the early-age behavior of BCOs on JCPs subjected to climatic loading, which results from temperature changes and moisture movement. To accomplish both of these objectives, an experimental BCO on JCP section was constructed and its concrete strains, temperatures, and the interfacial vertical and axial displacements were monitored. In addition, all other supporting data needed to calibrate the mechanistic delamination model, such as the climatic conditions, the pavement design, the material properties and the construction procedural information was collected. Two- and three-dimensional finite element models for the BCOs on JCPs were developed to represent the experimental sections. Using the results from these calibrated models, the delamination model already in HIPERBOND, NSLIP 2000 (Vallabhan et al., 1990; Nelson and Rasmussen, 2002), was modified to reflect the findings of this research. A sensitivity analysis of the modified delamination model clearly shows how various materials and construction variables influence the behavior of BCOs on JCPs.

2. Experimental study

To calibrate the mechanistic delamination model, an actual BCO on JCP used by the traveling public was initially going to be instrumented. However, to measure the vertical and axial displacements at the interface between the BCO and the existing pavement, the researchers had to be assured that delamination would occur. Because of the intrusive nature of this calibration plan, an experimental section that closely resembles a JCP overlay project was constructed instead. Strain gages, thermocouples, and linear variable displacement transducers (LVDTs) were installed. Climatic conditions were monitored at the time of construction, and the concrete material properties were measured in the laboratory.

2.1. Construction

Plan and profile views of the BCO on JCP are shown in Fig. 1. The BCO on JCP was constructed in two stages. First the JCP was placed and then the overlay. On June 18, 2001, the construction site was prepared. The section was excavated three inches with a backhoe, and wooden forms were placed around its perimeter using a surveyor's level. The JCP was placed on June 19, 2001. Ready-mix trucks arrived at 1:00 PM and the concrete was placed using hand pour equipment, like rakes and shovels. Concurrent with the construction process, concrete cylinders were prepared for testing in the laboratory. The JCP was finished with a roughly tined surface, except for a small 1.83 m by 1.83 m triangular section at midslab. This triangular portion was troweled smooth to ensure the overlay would delaminate from the existing pavement at this

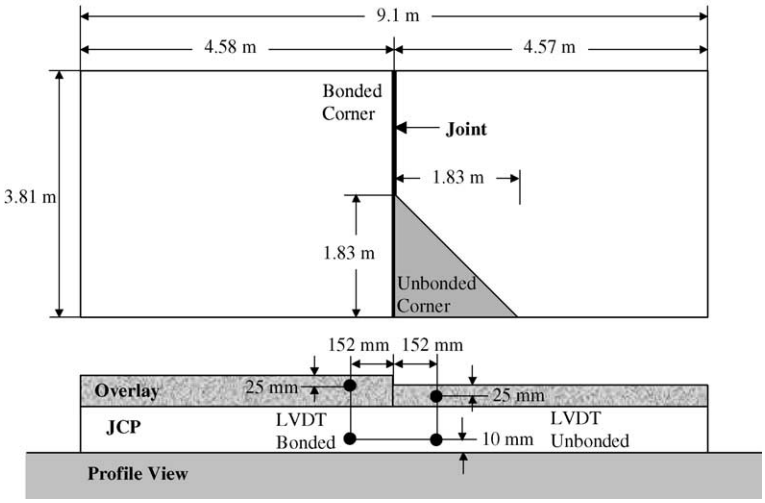

Fig. 1. BCO on JCP experimental section.

location. A transverse joint was scored at midslab during the finishing process. Ice had to be placed on the JCP to force the joint to form; ice creates a large temperature differential through the pavement thickness.

The BCO was placed during the afternoon of July 5, 2001, 17 days after the JCP was constructed. To maximize the interfacial bond strength between the BCO and JCP, all dirt and debris was removed from the JCP's surface. However, the smooth triangular section near midslab, referred to as the unbonded corner, was covered with plastic sheeting to guarantee no bond formed. A midslab joint was notched in the overlay after set. This joint formed the next day.

2.2. Instrumentation

A variety of sensors were installed before, during, and after the construction of the BCO on JCP to monitor its early-age behavior. Vibrating wire strain gages (VWGs) were embedded at three different depths in both the longitudinal and transverse directions in the unbonded and bonded corners as shown in Fig. 2a. These gages were attached to wooden dowels secured in the subbase. T-type thermocouples were also installed at varying depths at each of the instrumented corners, as shown in Fig. 2b. They measure the concrete temperatures. LVDTs were placed along the edge of the structure near midslab, as depicted in Fig. 1. LVDTs are designed to monitor the overlay's vertical movement, which is the result of differences in the overlay's and underlying JCP's thermal gradients and coefficients of thermal expansion (CTE). The day after construction, Demec studs were installed on the surface of the overlay to measure joint movement. A Pundit pulse-velocity apparatus was used to monitor the development of the concrete's mechanical properties and to estimate set time. A portable weather station was also installed on site to record climatic conditions.

2.3. Field data analysis

Pavements expand and contract as a function of temperature after the concrete has set. Similarly, slab curvature depends on the slab's temperature gradient at set. The set times of the overlay and JCP were determined by analyzing of the strains measured by the vibrating wire gages (VWGs) embedded in the concrete. Set was assumed to have occurred when the gage strains were consistently a function of the gage

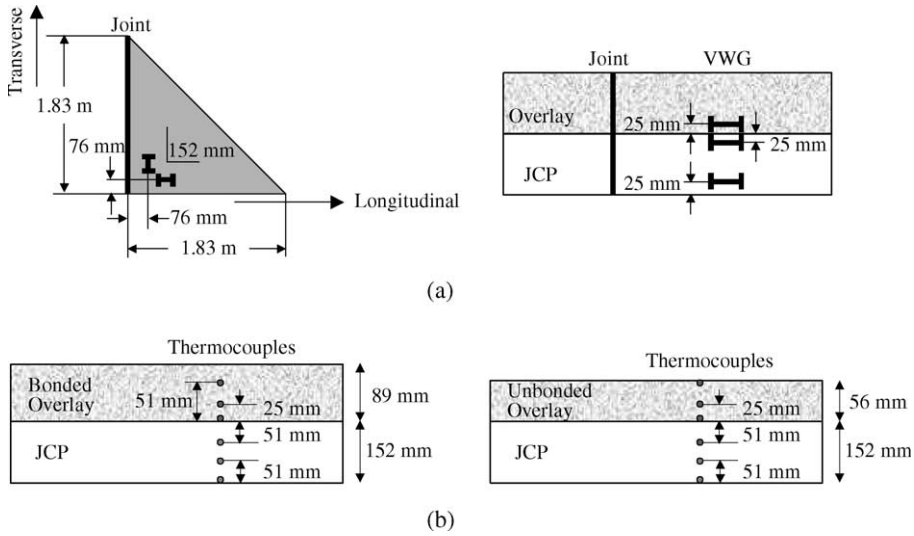

Fig. 2. Gage installation: (a) vibrating wire strain gages and (b) thermocouples.

temperatures. Set times were determined at each of the three VWG depths, and they were correlated to the thermocouple temperatures to obtain the set temperature profile. From this analysis, the concrete set approximately 4 h after it was placed, which is typical of hot weather concreting.

The LVDTs measure the vertical displacement of the unbonded and bonded corners from the existing JCP. The bonded corner is expected to adhere to the underlying JCP. Very little or close to no vertical or horizontal movement should be measured as the concrete temperature fluctuates throughout the day. The unbonded section of the overlay, on the other hand, is expected to separate from the underlying pavement. It will displace vertically and horizontally. The two LVDTs (one on the bonded corner and one on the unbonded corner) were placed several hours after the concrete set. This means that the initial movement recorded by the LVDTs does not necessarily represent full contact between the overlay and the underlying pavement. The LVDT readings will, however, indicate the relative vertical movement of the overlay from the underlying pavement. Fig. 3 shows the vertical displacements measured by the LVDTs for the bonded and unbonded corners. The vertical movement between the bonded corner of the overlay and the JCP is approximately zero, while there is significant movement between the unbonded corner of the overlay and the JCP. The unbonded corner has lifted off of the underlying pavement and no longer contacts its, as the daily cycles of vertical movement demonstrate. The overlay's permanent separation from the JCP is attributed to newly placed overlay's drying shrinkage. The vertical movement of the bonded corner increases at about three days meaning its interfacial bond has begun to fail.

To properly model the increase in vertical movement between the unbonded corner and the underlying JCP, the temperature profiles through the overlay and existing JCP were analyzed. Their effective temperature gradients were calculated using the following equations:

$$\mathrm{ETG}_{\mathrm{O}\,i} = \mathrm{TG}_{\mathrm{O}\,i} - \mathrm{TG}_{\mathrm{O\,set}} \tag{1}$$

$$\mathrm{ETG}_{\mathrm{JCP}\,i} = \mathrm{TG}_{\mathrm{JCP}\,i} - \mathrm{TG}_{\mathrm{JCP\,placed}} \tag{2}$$

where $\mathrm{ETG}_{\mathrm{O}\,i}$ is the effective temperature gradient in the overlay at time i; $\mathrm{TG}_{\mathrm{O}\,i}$, temperature gradient in the overlay at time i; $\mathrm{TG}_{\mathrm{O\,set}}$, temperature gradient in the overlay at set; $\mathrm{ETG}_{\mathrm{JCP}\,i}$, effective temperature

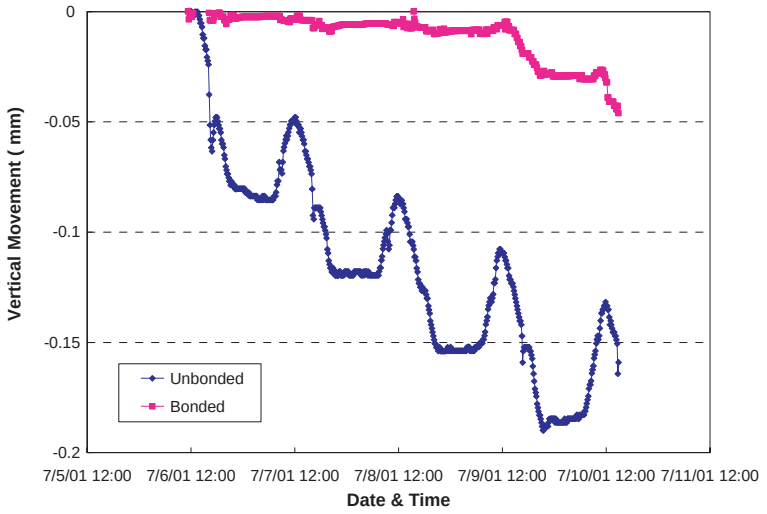

Fig. 3. LVDT readings for the bonded and unbonded corners.

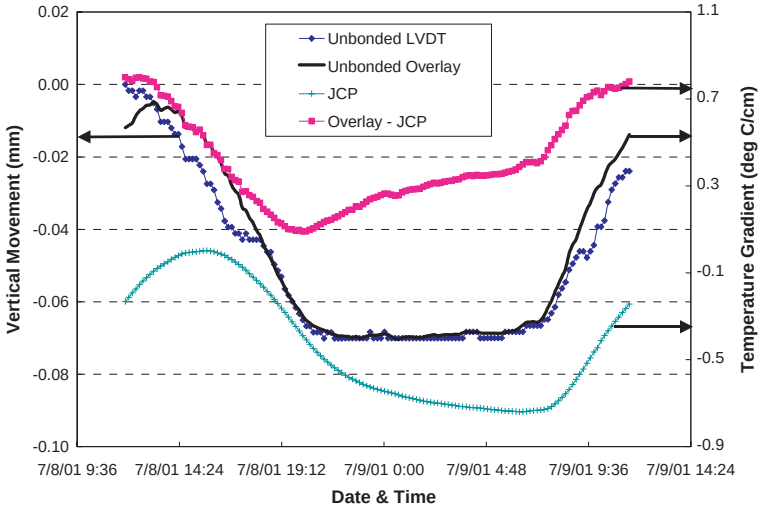

Fig. 4. Relationship between relative vertical movement and temperature gradients.

gradient in the JCP at time i; $TG_{JCP\,i}$, temperature gradient in the JCP at time i; and $TG_{JCP\,placed}$, temperature gradient in the JCP when the overlay was placed.

The time histories of the temperature gradients in the overlay (ETG_O) and in the JCP (ETG_{JCP}) and the differential temperature gradient between the overlay and the JCP ($ETG_O - ETG_{JCP}$) are plotted in Fig. 4 alongside the vertical movement of the unbonded section measured by the LVDT. In the figure, a negative temperature gradient means that slab surface is cooler than the slab bottom. The temperature gradient time histories match the shape of unbonded overlay's vertical movement closely, with the overlay's temperature gradient curve matching it very well. The temperature gradient in the overlay greatly influences interfacial separation.

To assess how the temperature gradients in the overlay and the JCP influence the vertical separation at the interface, a comparison plot was made (Fig. 5a). The temperature gradients and LVDT data were extracted from the readings on July 7 and 8, 2001, the time period when the relative vertical movement reaches its maximum value. When there is no vertical movement, the overlay is slightly curled down (ETG_O is about 0.2 °C/cm). As the vertical movement increases, the overlay's temperature gradient becomes more negative as it curls up. The JCP is initially in the curled up or flat shape for a vertical movement between 0 and −0.04 mm. When the vertical movement increases, the temperature gradient through the JCP becomes more negative meaning the pavement has a more significantly curled up shape. A plot of the differential temperature gradient ($ETG_O - ETG_{JCP}$) versus vertical movement is shown in Fig. 5b. As the differential temperature gradient decreases, the vertical movement increases. The relationship appears to be almost linear. These LVDT readings will be used to calibrate and validate the numerical delamination model

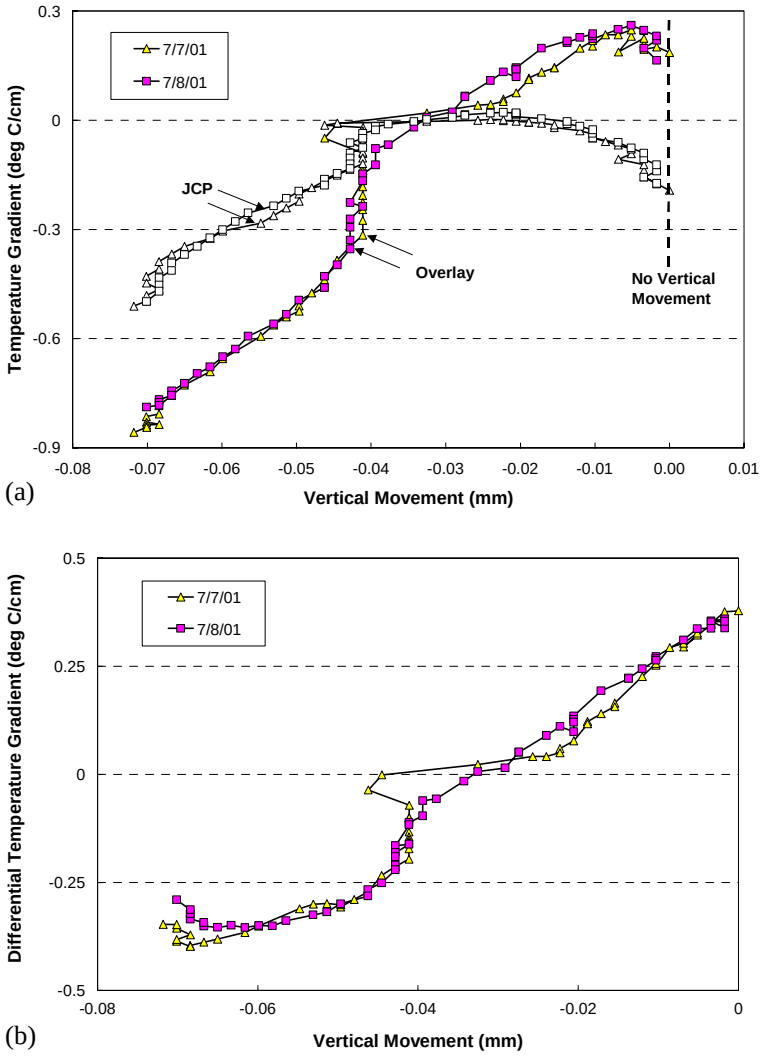

Fig. 5. Relative vertical movement in relation to: (a) the temperature gradient and (b) the differential temperature gradient.

presented in the next section; other experimental results from this study are not presented in this paper but elsewhere (Ruiz et al., 2001).

3. Numerical analysis

Two mechanisms can lead to delamination, namely, bond shear failure and bond tensile failure. These failure mechanisms can work independently or simultaneously. The end result is the same, namely the separation of the Portland cement concrete (PCC) layers. The first mechanism, bond shear failure, is caused by differential lateral movement between the two PCC layers. If the differential movement is great enough, the shear stress at the bond interface will exceed the bond shear strength, and a failure will occur in shear along the interface. A differential movement in the vertical direction causes the second failure mechanism, bond tensile failure. If the differential movement is great enough, the tensile stress at the bond interface will exceed the tensile strength of the bond.

3.1. Finite element modeling

Two- and three-dimensional finite element models of the BCO on JCP system have been developed for this study and they are based on models from previous studies (Kim et al., 1998, 2000, 2003). The model solutions are obtained using the finite element analysis program ABAQUS (1998). Fig. 6 shows part of the three-dimensional (3D) model. For the JCP, the concrete slab is discretized using three-dimensional brick elements. The frictional bond slip that occurs at the interface between concrete and subbase layer is modeled using horizontal spring elements in the longitudinal and the transverse directions. The underlying layers are modeled using vertical spring elements. If any side of the concrete slab curls up, a gap can form between the slab and the subbase layer. To properly model this curling effect, tensionless vertical springs that can sustain only compressive forces are used. For the overlay, the concrete slab is modeled using brick elements. To find the stresses and strains at the interface between the overlay and JCP, interfacial elements are used. The interfacial elements contain spring elements in three independent directions: x, y, and z. The boundary conditions of the finite element model should be correctly defined to obtain viable results. At joints, there is no restraint on the concrete. At midslab, the vertical degree of freedom and the horizontal degree of freedom in the transverse direction exist.

The two-dimensional (2D) finite element model is shown in Fig. 7. This model can be obtained by eliminating degrees of freedom in the transverse direction from the 3D model. The concrete slabs, therefore, are discretized using 2D plane elements. Since the behavior of the BCO on JCP system is symmetric with respect to the vertical planes along the two centerlines of the slab when the system is subjected to climatic loading, quarter symmetry is used for the 3D model and half symmetry is used for the 2D model. However, symmetry cannot be used to model the behavior of the BCO on JCP system that has an unbonded corner since that system is not symmetric.

3.2. Three-dimensional analysis

The experimental LVDT readings (relative vertical displacements) between the overlay and the existing JCP were used to calibrate and validate the 3D finite element model. The collected data, such as temperatures through the depth and material properties, at a selected time (July 8, 2001 at 22:51 in this study) was used as inputs for the numerical analysis. It is noted that the relative vertical displacements caused by creep and drying shrinkage of concrete were assumed to be very small compared with those caused by temperature changes within the period of a daily half-cycle of the displacement variation. Fig. 8 shows the relative

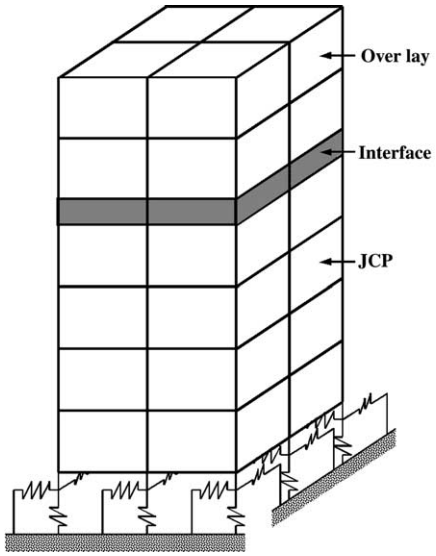

Fig. 6. Three-dimensional finite element model for BCO on JCP.

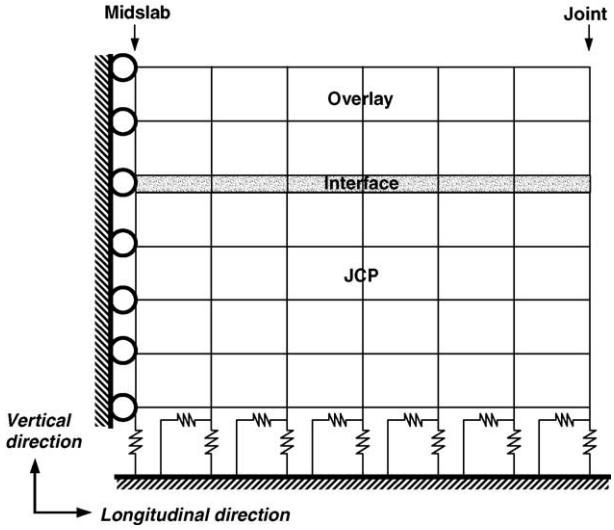

Fig. 7. Two-dimensional finite element model for BCO on JCP.

vertical displacements from the field experiment and the 3D finite element models. The result from the 3D finite element model with the tensionless springs for underlying layers is very close to the experimental result. Because of the curling action of the JCP, there will be very little or no bond in the vertical direction at the interface of the concrete slab and the underlying subbase. As mentioned previously, the 3D model with the tensionless springs for underlying layers can properly simulate this failure to bond in the vertical direction. The analysis results predicted by this model show that the vertical stiffness of underlying layers does not significantly affect the results (Fig. 8). Although the vertical stiffness of underlying layers at the

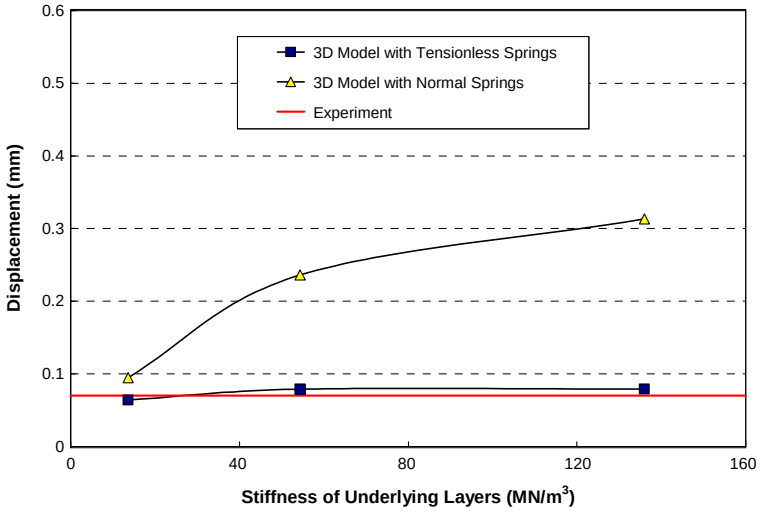

Fig. 8. Comparison between experimental and numerical analysis results.

experimental site was not measured directly (it was estimated to be very low between 15 and 30 MN/m^3), it is not a problem to compare the experimental result with the numerical analysis results because the vertical stiffness of underlying layers does not greatly affect the numerical analysis results.

A much simpler model for the underlying layers is to use normal springs instead of tensionless springs. If normal springs are used to model the underlying layers, the vertical relative displacement becomes larger as the vertical stiffness of underlying layers increases, as shown in Fig. 8. Similar results can be observed for the interfacial shear and normal stresses, as shown in Fig. 9. The finite element model with normal springs can significantly overestimate the relative vertical displacements and interfacial stresses when the stiffness of the underlying layers increases. However, if a low vertical stiffness value is used in the model with the normal springs, regardless of the actual stiffness value of underlying layers at the site, the finite element model with the normal springs can be used to predict the interfacial behavior of the BCO on JCP.

The effect of slab length (or joint spacing) on the interfacial stress has been investigated and the results are shown in Fig. 10. The maximum interfacial shear and normal stresses occur at the corner of the slab and are not affected by slab length. Significant stress changes can only be observed near the corner. It is noted

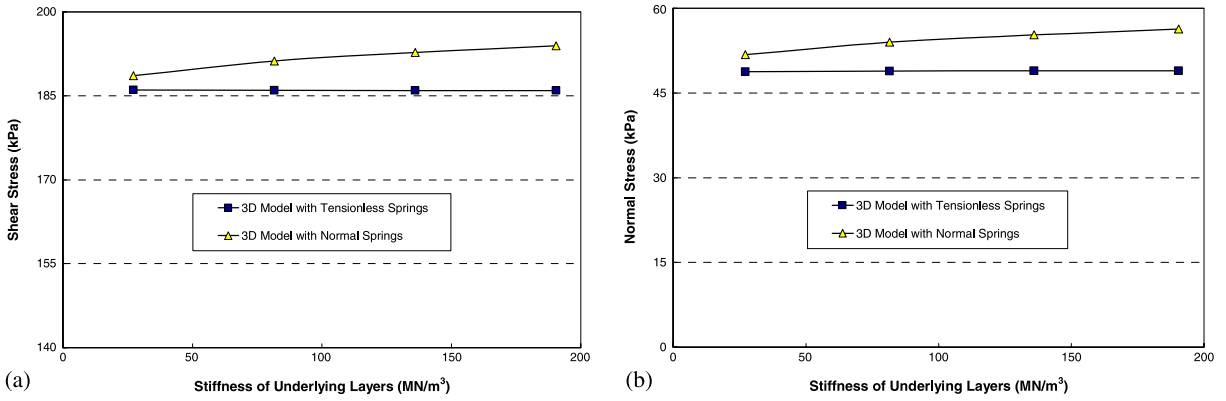

Fig. 9. Interfacial stresses from different 3D finite element models: (a) shear stresses and (b) normal stresses.

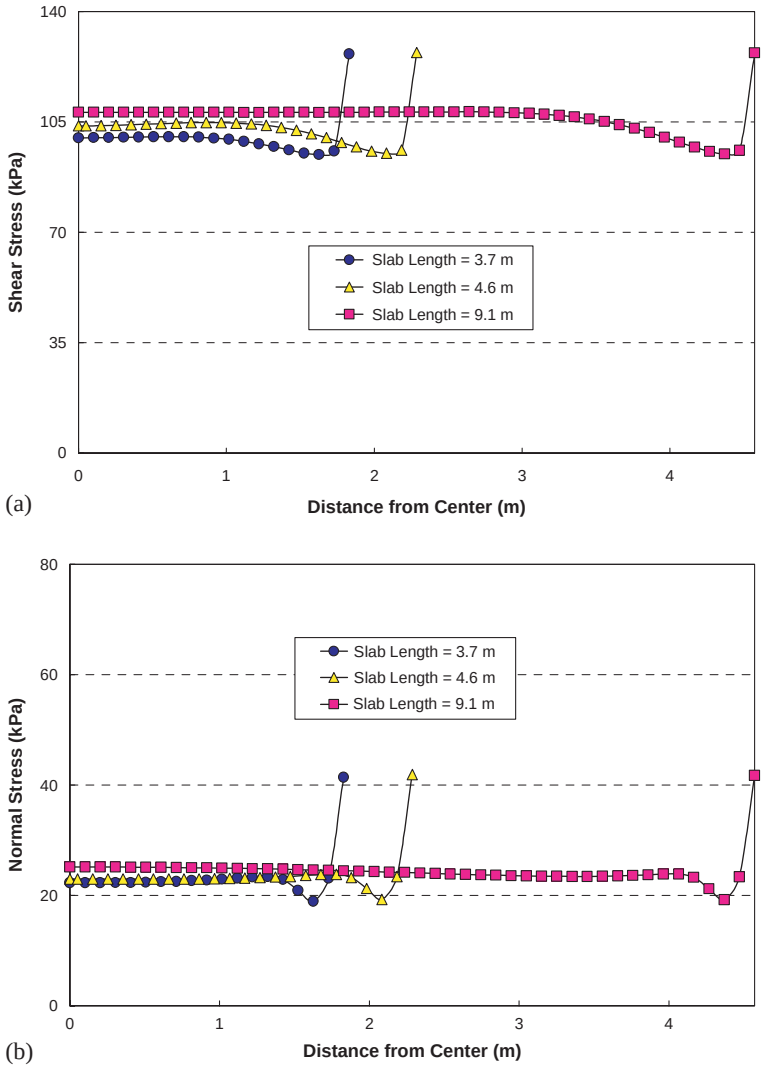

Fig. 10. Effect of slab length on interfacial stresses along the slab edge: (a) shear stresses and (b) normal stresses.

that the shear stresses are calculated as the vector sum of the shear stresses in the longitudinal and transverse directions.

3.3. Comparison between 2D and 3D analyses

Fig. 11 shows a comparison between the shear and normal interfacial stresses computed with the 2D finite element model and those computed with the 3D finite element model. The interfacial shear and normal stresses along the midslab obtained with the 3D model are very similar to those obtained with the 2D models. The stresses from the 2D model with plane strain elements are slightly higher than the stresses from the model with plane stress elements. The interfacial stresses along the edge obtained with the 3D model are very different from the 2D analysis results.

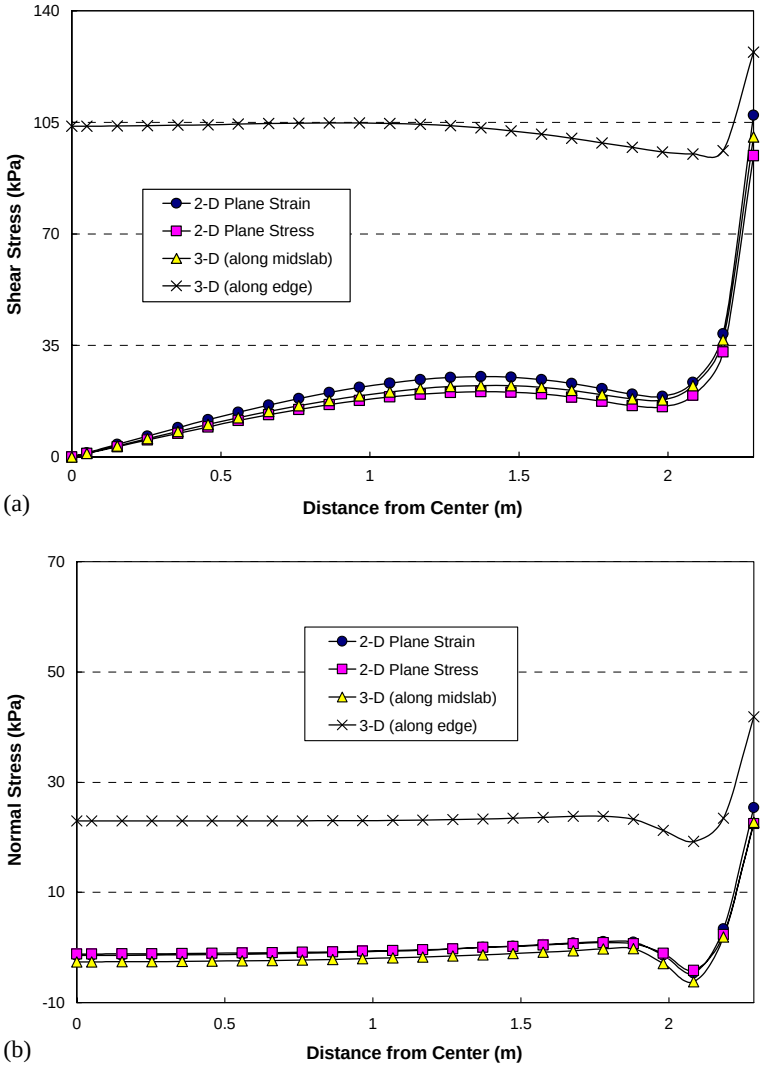

Fig. 11. Two- and three-dimensional analysis results: (a) interfacial shear stresses and (b) interfacial normal stresses.

Eqs. (3 and 4) have been developed from the results of a large number of analyses to relate, as best as possible, the shear and normal stresses obtained using the 2D model to those obtained using the 3D model at the slab corner.

$$\tau_{\text{corner}} = \sqrt{A_\tau^2 + B_\tau^2} \tag{3}$$

$$\sigma_{\text{corner}} = A_\sigma + B_\sigma \tag{4}$$

where τ_{corner} = maximum interfacial shear stress at the corner, σ_{corner} = maximum interfacial normal stress at the corner, A_τ = maximum interfacial shear stress from the 2D model along the longitudinal direction;

A_σ = maximum interfacial normal stress from the 2D model along the longitudinal direction, B_τ = maximum interfacial shear stress from the 2D model along the transverse direction, and B_σ = maximum interfacial normal stress from the 2D model along the transverse direction.

To obtain B_τ and B_σ, another 2D model has to be created in the transverse direction. The slab length of this model should be the width of the slab. Then, B_τ and B_σ are the maximum interfacial shear and normal stresses, respectively, obtained with this 2D model. The findings from the 2D and 3D analysis results have been integrated into the HIPERBOND program by modifying the current 2D finite element code for a BCO on JCP, NSLIP 2000 (Vallabhan et al., 1990; Nelson and Rasmussen, 2002).

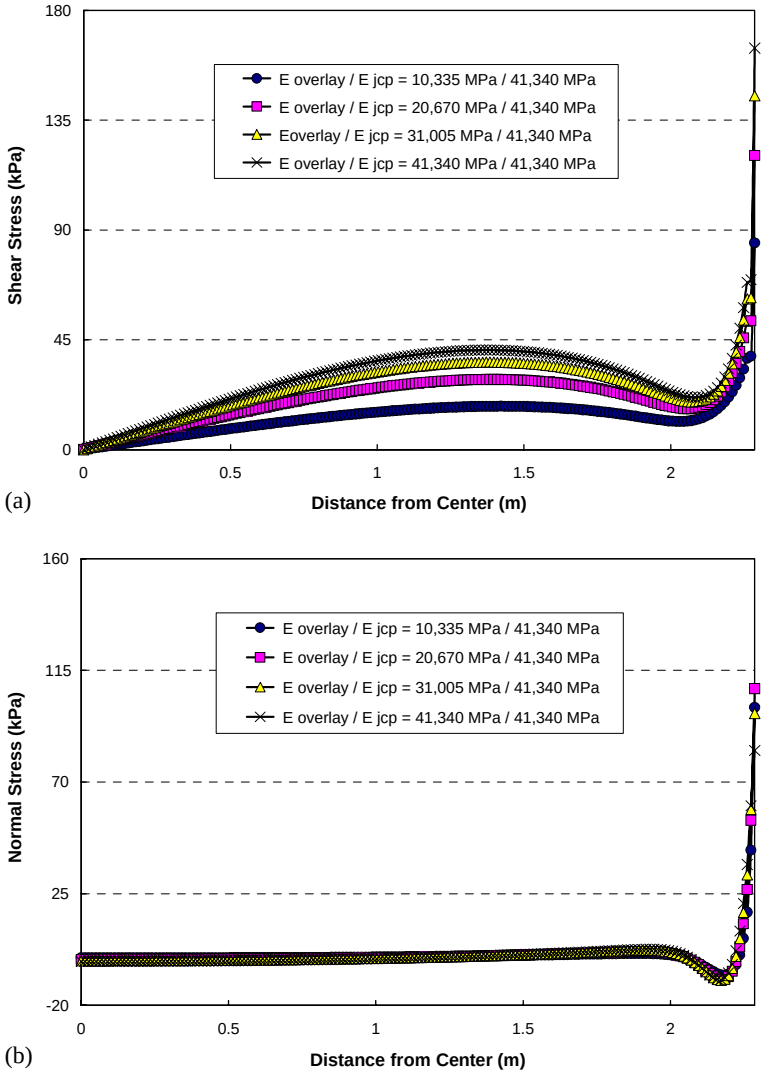

Fig. 12. Effect of elastic modulus of concrete on interfacial stresses: (a) shear stresses and (b) normal stresses.

3.4. Sensitivity study

A sensitivity analysis has been conducted with the 2D finite element model incorporated in HIPER-BOND to investigate the sensitivity of various parameters on the BCO on JCP shear and normal interfacial stresses. The control values of the model are as follows.

- Vertical stiffness of underlying layers = 54.4 MN/m^3 (200 psi/in)
- Elastic modulus of overlay = 20,670 MPa (3,000,000 psi)
- Elastic modulus of JCP = 41,340 MPa (6,000,000 psi)
- Thickness of overlay = 88.9 mm (3.5 in.)
- Thickness of JCP = 152.4 mm (6 in.)

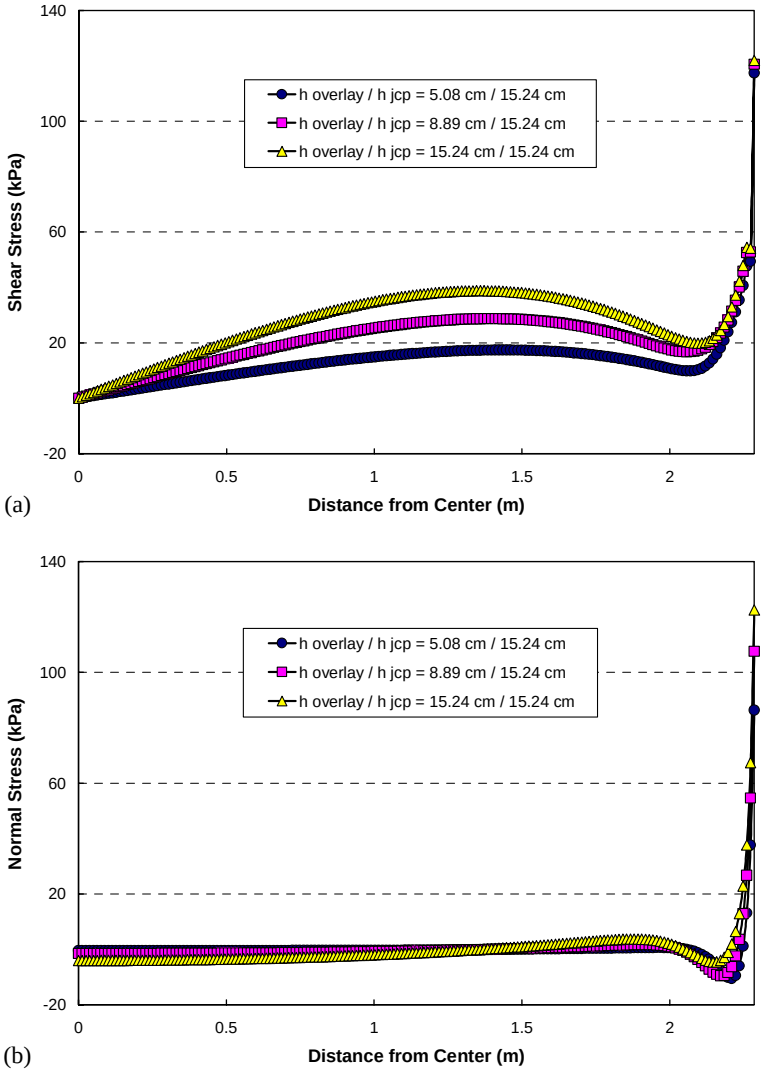

Fig. 13. Effect of thickness on interfacial stresses: (a) shear stresses and (b) normal stresses.

- Thermal expansion coefficient of overlay = 0.000007/°C, and
- Thermal expansion coefficient of JCP = 0.000006/°C

The effect of the overlay's elastic modulus on the interfacial stresses is shown in Fig. 12. The interfacial shear stresses increase as the elastic modulus of the overlay increases, as shown in Fig. 12a. The interfacial normal stresses, however, are not greatly affected by the ratio of overlay modulus to JCP modulus, as shown in Fig. 12b. Fig. 13 shows the effect of the overlay thickness on interfacial stresses. The interfacial shear stresses in the interior of the slab increase as the overlay thickness increases, but the maximum shear stresses at the joint or edge are almost the same (Fig. 13a). On the other hand, the interfacial normal stresses are almost zero in the interior of the slab, and the maximum normal stress that occurs at the joint or edge clearly increases with increasing overlay thickness (Fig. 13b). Fig. 14 shows the effect of the overlay's

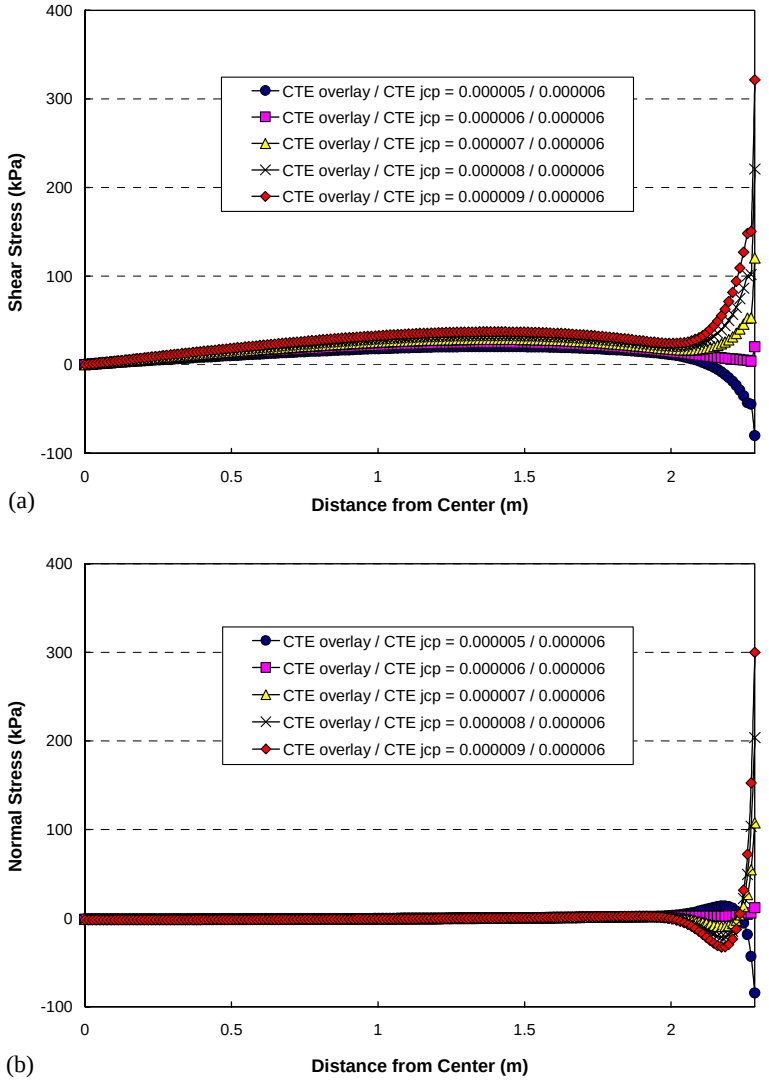

Fig. 14. Effect of concrete coefficient of thermal expansion on interfacial stresses: (a) shear stresses and (b) normal stresses.

coefficient of thermal expansion (CTE). The interfacial stresses near the joint or edge are greatly influenced by the ratio of overlay CTE to JCP CTE. As the CTE of the overlay increases, the maximum shear and normal interfacial stresses increase.

4. Summary and conclusions

To investigate the early-age behavior of bonded concrete overlays (BCOs) on PCC slab-on-grade pavements, an experimental BCO on JCP was constructed, instrumented, and monitored and a numerical analysis using finite element modeling was performed. The results from the experimental study were used to calibrate the numerical model. This model has been incorporated into the HIPERBOND software for a BCO on JCP. From this study, the following conclusions could be made.

- Daily vertical separation of the overlay from the underlying JCP at the slab edge seems to be caused primarily by the temperature gradient through the overlay.
- The relative vertical movement at the delaminated corner is almost linearly proportional to the differential temperature gradient between the overlay and the JCP.
- The 3D finite element model with tensionless springs for underlying layers predicts the experimental result well.
- The relative vertical movement and interfacial stresses between the BCO and JCP are overestimated using the 3D model with normal springs for underlying layers as the vertical stiffness of underlying layers increases. However, if a low vertical stiffness value is used, regardless of the actual stiffness value of underlying layers at the site, the finite element model with normal springs can still be used to predict the interfacial behavior of the BCO on JCP.
- A significant increase in the interfacial stresses occurs near the slab corner and edge. The slab length does not affect the predicted maximum interfacial stresses.
- The interfacial stresses obtained by the 2D finite element model represent the stresses along the midslab well.
- The interfacial stresses at the corner of the slab can be calculated using the 3D finite element model. They are larger than the edge stresses at midslab, as was expected since delamination initiates at the corner. Equations to predict the corner stresses using the 2D finite element model were developed.
- The interfacial shear stress increases as the elastic modulus of the overlay increases, however, the interfacial normal stress is not significantly affected by the elastic modulus.
- The interfacial shear stresses in the interior of the slab increase as the overlay thickness increases, but the maximum shear stresses are basically unchanged. The interfacial normal stresses are almost zero in the interior of the slab, but the maximum normal stress that occurs at the joint or slab edge increases with increasing overlay thickness.
- The maximum interfacial stresses are greatly influenced by the ratio of the overlay CTE to the JCP CTE. They become larger as the CTE of the overlay increases.

Acknowledgements

The authors gratefully acknowledge the support of FHWA under the project number DTFH61-00-P-00318. The authors would also like to thank Dr. R.O. Rasmussen, Mr. J.M. Ruiz, and Mr. D. Turner for their comments and help in conducting field experiments.

References

ABAQUS, 1998. User's manual version 5.8. Hibbit, Karlsson & Sorensen, Inc., Pawtucket, RI.

Kim, S.-M., Won, M.C., McCullough, B.F., 1998. Numerical modeling of continuously reinforced concrete pavement subjected to environmental loads. Transportation Research Record—Journal of the Transportation Research Board 1629, 76–89.

Kim, S.-M., Won, M.C., McCullough, B.F., 2000. Three-dimensional analysis of continuously reinforced concrete pavements. Transportation Research Record—Journal of the Transportation Research Board 1730, 43–52.

Kim, S.-M., Won, M.C., McCullough, B.F., 2003. Mechanistic modeling of continuously reinforced concrete pavement. ACI Structural Journal 100 (5), 674–682.

McCullough, B.F., Rasmussen, R.O., 1999a. Fast-track paving: Concrete temperature control and traffic opening criteria for bonded concrete overlays, Volume I—Final report. Report FHWA-RD-98-167, FHWA, Washington, DC.

McCullough, B.F., Rasmussen R.O., 1999b. Fast-track paving: Concrete temperature control and traffic opening criteria for bonded concrete overlays, Volume II—HIPERPAV user manual. Report FHWA-RD-98-168, FHWA, Washington, DC.

Nelson, P.K., Rasmussen, R.O., 2002. Delamination stresses at the interface of bonded concrete overlays. In: Proceedings of the 81st Annual Meeting of the Transportation Research Board. National Research Council, Washington, DC.

Ruiz, J.M., Rasmussen, R.O., Nelson, P.K., Chang, G.K., Dick, J.C., Turner, D.J., 2001. Bonded concrete overlay: Behavior prediction model enhancement and calibration for CRCP. Report DTFH61-00-P-00318, The Transtec Group, Inc., Austin, TX.

Vallabhan, C.V.G., Asik, M., Rahman, K., 1990. A finite element program for analysis of bonded concrete overlays. Report 1105-3, Texas Tech University and Texas Sta Department of Highways and Public Transportation.